HHS Public Access

Author manuscript

Magn Reson Med. Author manuscript; available in PMC 2017 May 01.

Published in final edited form as:

Magn Reson Med. 2016 May ; 75(5): 2156–2164. doi:10.1002/mrm.25762.

Multi-Component T_2 Relaxation Studies of the Avian Egg

Dimitris Mitsouras[1], **Robert V. Mulkern**[1,2], and **Stephan E. Maier**[1,3]

[1]Department of Radiology, Brigham and Women's Hospital, Harvard Medical School, Boston, MA, 02115

[2]Department of Radiology, Children's Hospital, Harvard Medical School, Boston, MA, 02115

[3]Department of Radiology, Sahlgrenska University Hospital, Gothenburg University

Abstract

Purpose—To investigate the tissue-like multiexponential T_2 signal decays in avian eggs.

Methods—Transverse relaxation studies of raw, soft-boiled and hard-boiled eggs were performed at 3 Tesla using a 3D Carr-Purcell-Meiboom-Gill (CPMG) imaging sequence. Signal decays over a TE range of 11 to 354 ms were fitted assuming single- and multi-component signal decays with up to three separately decaying components. Fat saturation was used to facilitate spectral assignment of observed decay components.

Results—Egg white, yolk and the centrally located latebra all demonstrate nonmonoexponential T_2 decays. Specifically, egg white exhibits two-component decays with intermediate and long T_2 times. Meanwhile, yolk and latebra are generally best characterized with triexponential decays, with short, intermediate and very long T_2 decay times. Fat saturation revealed that the intermediate component of yolk could be attributed to lipids. Cooking of the egg profoundly altered the decay curves.

Conclusion—Avian egg T_2 decay curves cover a wide range of decay times. Observed T_2 components in yolk and latebra as short as 10 ms, may prove valuable for testing clinical sequences designed to measure short T_2 components, such as myelin-associated water in the brain. Thus we propose that the egg can be a versatile and widely available MR transverse relaxation phantom.

Keywords

T_2-decay; CPMG; multiexponential; egg white; yolk; latebra; MR phantom

Introduction

The common unfertilized chicken egg is one of the richest sources of protein available, supplying the raw material from which the tissues of the animal are formed (1,2). The raw egg is practically a liquid, with both the white and yellow yolk spreading out on a flat surface – the white more so than the yolk. Cooking introduces clear textural differences

Address correspondence to: Stephan E. Maier, MD, PhD, Radiology (MRI), Brigham and Women's Hospital, Harvard Medical School, 75 Francis Street Boston, MA 02115, Tel: 617 - 732-5065, Fax: 617 - 264-5275, stephan@bwh.harvard.edu.

between raw, soft-boiled (SB) and hard-boiled (HB) eggs. As Michael Pollan notes in his book “Cooked: A Natural History of Transformation” (1), the cooking process of an egg increases the digestive capacity from 65% to 95%. The white of the soft-boiled egg is capable of holding an ovoid shape against gravitational forces when removed from the shell. However, the yolk in the interior remains gooey. The hard-boiled egg presents yet a different texture, with a firmer overall feel, and a yolk that is somewhat “chalky” and readily crumbles into yellowish and/or dark fragments. Previously, we examined the water and lipid diffusion properties of the egg white and yolk in raw, SB and HB eggs, and characterized the diffusion properties of the less well-known latebra (3), a small structure clearly visible within the yolk on T2-weighted MR images. In the present work we continue the characterization of the MR properties of the egg white, yolk and latebra with detailed studies of transverse relaxation decay properties in their raw, SB and HB conditions.

Utilizing 3D Carr-Purcell-Meiboom-Gill (CPMG) imaging sequences following the basic principles set out by Poon and Henkelman, we obtain high signal-to-noise ratio (SNR) T_2 decay curves (4,5) wherein stimulated echo effects are minimized (6,7). The resulting decays enable arguably unambiguous assessment of multiexponential functions describing the individual signal decay curves in each of the three major structures in raw, SB and HB eggs. Additional experimental manipulations via the application of fat saturation (FS) pulses further elucidate features of the multiexponential T_2 decays and associations between the observed components. A conceptual effort to link the findings to previously-reported diffusion studies is made, as well as suggestions as to how the transverse relaxation properties of the egg may be deployed as phantom material in the development of clinical techniques devoted to extracting information from short T_2 components such as myelin associated water, a potentially important biomarker of disease (8-11).

Methods

Specimen Preparation

Raw unfertilized chicken eggs were purchased at local groceries. Imaging and relaxometry studies were performed in raw eggs (n=3), 5-min SB eggs (n=3) and 15-min HB eggs (n=3). All eggs were allowed to equilibrate to scanner room temperature for approximately 24 hours prior to scanning.

Magnetic Resonance Imaging Equipment

Experiments were performed on a 3 Tesla GE HDx MR whole-body imager (General Electric, Milwaukee, WI), equipped with gradients capable of 40 mT/m amplitude and 150 T/m/s slew rate. A birdcage wrist coil was used for radiofrequency (RF) signal reception.

MR Transverse Relaxation Sequence

A 3D non-selective multi-echo Carr-Purcell-Meiboom-Gill (CPMG) imaging pulse sequence was used to acquire transverse relaxation decay curves (4). The sequence resembles a fast-spin echo (FSE) sequence except that each echo of the echo train is identically encoded by a single phase- and slice-encoding step immediately after the tip-down pulse, rather than with repeated encoding and rephasing around each echo. Moreover, two modifications were

added to enhance the accuracy of transverse relaxation measurements (5). These modifications ensure that stimulated and indirect signal echo pathways that are T_1 relaxation-dependent (7) are (a) minimized, (b) suppressed, or (c) appear as a mirror image of the imaged object.

The first modification involves the use of composite, 90_x-180_y-90_x refocusing RF pulses. These composite pulses achieve refocusing flip angles close to 180° over a wider range of B_1 (transmit) and B_0 (main) magnetic field inhomogeneities compared to standard (slab- or non-selective) 180_y refocusing RF pulses, thereby minimizing indirect and stimulated echo formation. The second modification consists of symmetric spoiler gradients before and after each refocusing RF pulse wherein the signal dephasing imparted is varied from pulse to pulse by linearly stepping down the gradient amplitude after each echo and by alternating the polarity of the gradient after every second echo. With this modification, stimulated and indirect echo pathways, even if formed, have a very low likelihood of refocusing. The amplitudes and durations of the first and last spoiler were designed to impart 25π and 1.56π phase dispersal, respectively. Furthermore, because phase encoding along two directions is performed once immediately after the tip-down pulse, insufficiently crushed indirect and stimulated echo pathways will be encoded with reverse polarity at either odd or even readouts compared to that of the direct echo. In the final image, this causes a mirror of the object to appear (in either the phase or slice-encode dimension), which, provided a suitable a field-of-view is selected, will not overlap with the object of interest.

Each egg was imaged with this sequence in a separate scan. With each scan, a total of 32 echoes (3D volumes) were collected at equally spaced echo times ranging from approximately 11 to 394 ms with an echo spacing between 11 and 13 ms, and a 3 sec repetition time (TR). For all specimens, resolution was 1.33×1.33×2.00 mm^3 with a 96 (readout) × 72 (phase) × 50 (slice) matrix, covering a field-of-view (FOV) of 128×96×100 mm. Signals were acquired without averaging (NEX=1). These settings resulted in a scan time of 180 min. The duration of the 90° non-selective tip-down pulse was 500 μsec, and that of the composite non-selective refocusing pulse 1 ms; the receiver bandwidth was ±50 kHz with resulting in a 960 μsec readout time. To achieve sufficient dephasing, each wing of the gradient surrounding the refocusing pulses was 3-4 ms long, largely dictating the echo spacing.

The CPMG sequence was applied in two variations to each specimen; once without additional RF pulses, i.e., with no preparation (NP experiment); then with a fat saturation pulse performed prior to each excitation (FS experiment). For the FS experiments, the system-default, chemically selective saturation RF pulse (8 ms, 95° adiabatic RF excitation pulse of roughly 500 Hz full-width at half maximum) was applied at the default timing prior to the tip-down pulse, followed by a large spoiler gradient.

MR Image Analysis

A total of n=135 square regions of interest (ROI) were analyzed in the NP CPMG image data sets of the 9 eggs (white n=80, yolk n=48, latebra n=27), roughly equally distributed amongst eggs considering their variable size. ROI sizes ranged from 2×2 (latebra) to 10×10 (white) pixels. For each ROI, the identical ROI in the corresponding FS experiment of the

same egg was also analyzed. Signal decays in each ROI were fitted with mono-, bi-, and tri-exponential decay models (12) using an iterative non-linear nonnegative least-squares routine. Constraints were that each of the T_2 times must be greater than half of the echo spacing, and less than 2 seconds. The algorithm and a graphical user interface were implemented in Matlab (Matlab R2008b, Mathworks, Natick, MA). The monoexponential fit yielded a single (bulk) T_2 decay time, whereas the biexponential and triexponential fits yielded respectively two (short and long) and three (short, intermediate, and long) T_2 decay times, as well as their respective relative signal fractions.

Statistical Analysis

Goodness-of-fit was assessed with chi-squared (X^2) values. Specifically, an *F*-test was used to determine if any reduction in X^2 was statistically significant relative to the differences in degrees of freedom for each of the three fits (mono-, bi-, or triexponential). In the *F*-test, the ratio of variances (*F*-ratio) is converted by the *F*-cumulative distribution function to yield the probability *p* of type I error (rejection of a true null hypothesis). A significant *p* value implies that, e.g., a bi-exponential fit is statistically more appropriate than a mono-exponential fit, or a tri-exponential more appropriate than a bi-exponential fit (13). Comparison of mean fitted T_2 decay times measured with the different experiments (NP vs FS) as well as for each of the three structures across specimens at each condition was performed using the unpaired Student *t*-test or one-way analysis of variance (ANOVA) as appropriate. A *p* value of <0.05 was considered statistically significant.

Results

Sample images at four different echo times are shown in Fig. 1 for each of the three egg preparation states. Transverse relaxation curves from all three structures demonstrated either biexponential or triexponential behavior, irrespective of raw or cooked condition. Note some inhomogeneity in the white of the SB egg, indicating cooking from the outside in. In such cases, ROIs encompassing the entire region of the egg white were selected. Table 1 reports the relaxation times and relative signal fractions for the egg white, yolk and latebra for the raw, SB, and HB conditions, and for each of the two sequence setups, i.e. NP and FS. The ensuing discusses each structure in detail.

Egg White

On semi-log plots over the range of TE values, transverse relaxation decay curves from egg white appeared rather linear (Fig. 2). More careful inspection of residual plots (Fig. 2) however revealed a slight deviation from monoexponential decays, indicating that a multiexponential model may be more adequate. Statistical support for bi- rather than mono-exponential functions for all egg white decay curves was provided by *F*-tests; the *F*-ratio for mono- vs biexponential across all conditions was >198.5 (average: 1095.1) and >121.4 (average: 1669.7) for NP and FS experiments, respectively. Triexponential fits were not supported, except for some of the ROIs in raw eggs (note the slight fluctuation in the biexponential fit residual at 60 and 110 ms TE in Fig. 2B), possibly indicating an additional short component not generally resolvable under the conditions of our experiment. The biexponential analysis of T_2 decay curves of raw egg white revealed a minor (14%) fast

relaxing component with a T_2 of approximately 65±4 ms and a dominant (86%) slowly relaxing component with a T_2 of approximately 218±11 ms. Cooking invoked a substantial decrease of the fast relaxation time by about 30% and a dramatic decrease of the slow relaxation time by about 70%. At the same time the relative signal fraction of the fast relaxing component increased from 14% to around 34-40% and, vice versa, the slow relaxing component decreased from 86% to around 60-67%. Fat saturation entailed a significant increase of the fast relaxation time in raw and SB egg white only. Meanwhile, also in raw and particularly in SB eggs, fat saturation caused a significant shift of the relative signal fractions towards a larger fast-relaxing fraction. For eggs with identical preparation and experimental setup, there were no statistically significant differences (ANOVA $p>0.06$-0.94, depending on condition and experiment), except for the HB white for which one of the 3 specimens presented 9 to 11 ms higher T_2 times compared to the other two eggs (ANOVA $p<0.002$ for both the short and long NP and FS T_2 times).

Yolk

Yolk transverse relaxation decay curves were clearly non-monoexponential. *F*-tests of multiexponential fits revealed that under most conditions, triexponential functions best characterized yolk transverse relaxation, though biexponential functions were more appropriate under some specific conditions (see Fig. 3B-D). Specifically, in raw yolk, triexponential functions appeared most appropriate (average *F*-ratio for tri- vs. biexponential, 35.1, range: 5.5-103.6), with fast, intermediate and slow T_2 times of approximately 13±2 ms, 23±2 ms, and 288±51 ms, and respective relative signal fractions of roughly 39%, 59% and 2%. In SB yolk, biexponential functions appeared more appropriate than triexponential functions (average *F*-ratio for tri- vs. biexponential, 0.7 range: 0-2.8). The overwhelming fast relaxing component (98% signal fraction) presented a T_2 decay time of about 18±1 ms. This is in good agreement with the signal-fraction weighted average of the fast and intermediate relaxation times observed in raw eggs (18.5 ms) and HB eggs (18.8 ms). The slow relaxation component fraction of SB yolk was in consensus with that in raw eggs (2%), but the T_2 relaxation time of 105±16 ms was significantly shorter. In HB yolk, as in raw yolk, triexponential functions resulted in the best fits (average *F*-ratio, 15.7, range: 5.5-62.4), with fast, intermediate and slow T_2 relaxation times of approximately 13±1 ms, 37±3 ms, and 81±10 ms, and respective relative signal fractions of around 67%, 27% and 6%. Notable in comparison to raw yolk is an apparent exchange of the fast and intermediate relative signal amplitudes (fractions of 67% and 27% in HB yolk vs 39% and 59% in raw yolk), in conjunction with higher intermediate and lower slow T_2 relaxation times. Also remarkable in comparison to raw and SB yolk, is a three-fold significant increase of the slow relaxing signal fraction in the HB state.

With fat saturation, biexponential fits were most appropriate for all yolk preparations (see Fig. 3C-D). Fat saturation also caused a significant reduction of the yolk's fast T_2 relaxation time in all states (raw −14%, SB −35%, and HB −28%). It should be noted that the decrease was most dramatic for SB yolk, where, unlike raw and HB yolk, the optimal fit for the NP experiment was also biexponential. Indeed, with fat saturation, yolk fast T_2 relaxation times became alike at all preparations. Moreover, a significant increase of the slow relaxation time was observed only in HB yolk with fat saturation. Also remarkable was that after fat

saturation, relative signal fractions for raw, SB and HB yolk became similar, i.e., around 97% and 3%, for the fast and slow relaxing signal fraction, respectively. There were no statistically significant differences across eggs with the same cooking condition for either the NP or FS experiments (ANOVA p>0.05—0.78, depending on condition and experiment).

Latebra

Curvature on the semi-log signal decay plots indicated clearly non-monoexponential decays in the latebra (Fig. 4). For all experimental variations, the multiexponential character of the latebra decay curves was best described by triexponential functions (average F-ratio across all conditions, 173.5 range: 13.0-796.6). The fast and intermediate relaxing component in raw, SB and HB eggs had T_2 values on the order of 15-19 ms and 50-55 ms, respectively. The slow relaxing component exhibited a greater variation; in raw eggs, it was on the order of 134±32 ms, becoming 148±16 ms and 105±7 ms in SB and HB eggs, respectively. The relative signal fraction of the intermediate component was consistently around 45%, while the relative signal fractions of the fast/slow relaxing component changed from 25%/29% in raw, to 33%/22% in SB and 24%/33% in HB eggs.

Fat saturation reduced the T_2 time of the fast relaxing component significantly, between 55% in HB and 35-38% in raw and SB eggs. The T_2 time of the intermediate component also diminished significantly in SB (-13%), and in HB (-20%) eggs. The only significant change of a relative signal fraction with fat saturation was a small decrease of the fast relaxing fraction in HB eggs.

There were again no statistically significant differences in either of the multi-exponential fitted T_2 times for the latebra across eggs at the same cooking condition for either the NP or FS experiments (ANOVA p>0.06—0.83, depending on condition and experiment).

The signal difference between NP and FS experiment was consistently best fitted with a biexponential decay (Fig. 5), whereby the faster characteristic decay time fell between the T_2 time of the fast and intermediate relaxing components and the slower characteristic decay time equaled the T_2 time of the slow relaxing component.

Discussion

Occasionally it is of interest, to some of us, to stop thinking of our expensive, state-of-the-art clinical scanners as simply tools for the practice of diagnostic radiology but rather as elegant instruments for performing sophisticated materials science studies of intact, biological objects such as the common egg, albeit usually on quiet Sunday afternoons in our MRI facilities. The “need for speed” clamored for in clinical studies can then be suspended, and scan times lengthened, to accommodate increased signal-to-noise ratios and the minimization of nuisance artifacts, such as signals from stimulated echoes, that otherwise hinder detailed transverse relaxation studies with CPMG imaging sequences. One may then query, of course, as to what end is the use of expensive clinical scanners for this purpose helpful to humanity? The primary response to this query lies in the value associated with the scientific challenge of matching, or reconciling, high quality experimental data with biophysical models of the underlying water and/or lipid proton signal components

responsible for this data. This is generally no easy task, but one that can only aid in translational “bench-to-bed” implications for the interpretation of clinical MRI examinations. A secondary response to this query would be that phantom materials for calibration experiments and testing of methods for extracting short T2 components, such as the myelin associated water (MAW) component in brain, are always valuable and indeed we believe the egg can provide such a material as we demonstrate further below. For now, however, and in deference to the primary response to the query, we attempt to explain the transverse decay curve data acquired from the three identifiable structures within the egg in terms of available physical and chemical models of this common but remarkable biological object.

Egg white

By weight, egg white is approximately 90% water and 10% proteins, the latter consisting of albumins, mucoproteins and globulins. In contrast to the yolk, there is little or no lipid content. Assuming monoexponential decays as a first (and often appropriate) approximation, it is remarkable that boiling of egg white for either 5 or 15 minutes results in a dramatic decrease, approximately four-fold, in the T_2 decay times. Decreases in T_2 are generally expected as the more liquid-like egg white is transformed by cooking into a more semi-soft solid material where one might expect significant decreases in the rotational and/or translational motions of individual water molecules. It is of further interest to note, however, that in our previous study of diffusion in egg white (3), we found that the reduction in the diffusion coefficient, D, in going from raw to either SB or HB states is rather small, on the order of 7%. Thus it appears that the cross-linking of the proteins to form the solid-like lattice of egg white results in an increase in the low frequency fluctuations responsible for T2 decay without altering the translational diffusion of the water molecules very much. Monoexponential analyses of T_2 decay in egg white proved insufficient, however, to fully characterize the observed decay curves in this work. It is likely that without the high signal-to-noise ratios achieved and the use of a CPMG sequence that minimizes systematic errors from B_1 and B_0 inhomogeneities, the biexponential decay would have remained unappreciated. The predominant component in both raw and cooked eggs was the slower decaying component, which in the former accounted for some 86%, dropping to ~60% of the signal in the latter. Cooking reduced the long T_2 value dramatically but also reduced the short T_2. The FS pulse did result in some small but significant changes of biexponential parameters characterizing the egg white decay curves despite the fact that egg white contains negligible fat. We speculate that this is due to a combination of direct saturation and MT effects though acknowledge that more detailed magnetization transfer studies would be required to better understand this phenomenon. As a guide to the potential involvement of these effects in this work, the relative change of proton density in the egg white with the FS preparation compared to no preparation was 2-5% across all three conditions.

The precise nature of the two T_2 components in egg white is not known. Furthermore, the fact that the decay curves accommodate two components does not preclude the possibility that a more complicated distribution of T_2 values may also account for the observed decay. We do note, however, that in our previous diffusion study of egg white over extended b-factors, a small slowly diffusing component at the higher b-factors in the cooked eggs could

not be discounted, suggesting that additional diffusion studies of egg white with higher SNR may help elucidate the nature of the two T_2 components.

Yolk

The chemical complexity of yolk obviously contributes to the composite, multiexponential T_2 decay curves we have observed. According to Stadelman and Cotterill (2), the yolk consists of approximately 50% water, 34% lipids and 16% proteins with other minor components made up of minerals and carbohydrates. In our studies of yolk T_2 decay curves, the most informative experiment that allowed us to unambiguously assign specific T_2 components to water or lipid protons arose from the fat saturation pulse preparations. Namely, the FS pulse obliterated the intermediate T_2 component of the triexponential curves in raw and HB yolks, rendering them biexponential decays with a very fast-relaxing, dominant T_2 component, and more slowly relaxing, much smaller, T_2 component. Thus we assign the second, or intermediate, T_2 component in triexponential T_2 decay curves of yolk to the methylene and methyl lipid protons, and the fastest and the slowest T_2 components to two additional distinct water pools. In the raw egg, these two water pools together accounted for some 42% of the percentage amplitudes, less than expected for a 60% water content of the water and lipid part of the yolk.

Hard boiling of the yolk increased the observed water percentage above 70%, more in keeping with the reported relative water content. In this study we utilized a 3 s TR which, for long water T_1 values on the order of 2 to 3 s in raw yolks, would have resulted in a saturation of the water signal, reducing its apparent percentage. A shortening of the water T_1 in the HB yolks could account for reduced saturation effects, and thus observed water percentages more in line with those expected from reported egg yolk chemical compositions. Further studies of the T_1 properties of the T_2 components are needed to validate this speculation, though this seems to be the most likely cause of the different apparent water contents in the two states. It is clear that hard boiling has an effect on the lipid T_2 values, raising them from ~23 ms to ~37ms. We note that Fieremans et al (11) reported that mild heat treatment of dairy cream phantoms prior to room temperature experiments resulted in prolonged lipid transverse relaxation times, as observed in our HB egg yolks. In the SB egg yolks, the T_2 decay curves exhibited biexponential as opposed to triexponential behavior. The fat saturation pulse in this case dropped the value of the fast T_2 component from ~18 ms to a value of ~12 ms, similar to that observed in the raw eggs. We attribute the biexponential behavior in SB eggs to a shortening of the lipid T_2 value towards that of the faster water T_2 value, resulting in an inability of our relaxation data to resolve these two components.

This speculation may be bolstered with future experiments using water as opposed to fat saturation pulses, but appears to be a reasonably plausible explanation of the data. Thus we speculate that in SB yolks, the fastest water T_2 values are similar to those observed in raw yolk but that the T_2 value of the primary methylene/methyl lipid protons is reduced from that in raw eggs. In HB eggs the situation is decidedly different, with the lipid T_2 values rising more than 50%. The crumbly vs gooey nature of the HB vs SB yolk clearly has profound effects on lipid T_2 values and we speculate that this may be a manifestation of lipid coagulation and sequestration from the water component in the former. Finally, we suspect

that in HB eggs, the third, slowly relaxing component is contaminated with a methyl proton signal with a prolonged T_2 value, a feature suggested by the reduction in amplitude of this component from ~6% to ~3% upon application of the fat saturation pulse. This feature is not evident in the raw or SB eggs where we speculate the third, slowly relaxing component is comprised solely of water.

Latebra

The latebra decay curves, arising from the smallest structure examined and embedded well within the yolk, most probably suffer from partial volume effects, with signal contributions from the yolk lipids. For example, fat saturation pulses reduced the signal from the first echo by ~16 to 24%, indicating perhaps the degree of partial volume effects. The decrease in the fastest component's T_2 from ~17 to ~10 ms with fat saturation in raw, SB and HB eggs is also consistent with the fastest component being water, as in the yolk. The fact that the second and third slowest decaying components were largely unaffected by the fat saturation pulse indicates that these two components arise from water protons. Given that their T_2 values are in the 49-55 ms and 105-148 ms range, respectively, these components most probably are the primary contributors to the multiple diffusion components we observed in our previous diffusion study in which relatively long echo times (>80 ms) were employed (3). The response of the triexponential parameters to cooking are somewhat complex, with fairly small changes in the actual T_2 values themselves, though in HB eggs the slowest decaying component shows a 15-25% lower T_2 value than raw or SB eggs, respectively.

Conclusion

We conclude with some comments regarding the suitability of eggs as a phantom material for assessing methods designed to more rapidly extract quantitative information regarding fast T_2 components such as myelin associated water (8-11) which may become an important biomarker of several disease processes in the brain. These comments must of course be considered in the context of the limitations of the sequence and our experimental conditions. Particularly at 3 Tesla, B{0,1} inhomogeneities can be quite large and thus a significant proportion of the magnetization may follow indirect and stimulated echo pathways. The resulting signal loss across the length of the echo train may thus yield an artifactual T_2 decay. However, by using composite refocusing pulses and a small FOV, loss of signal to those pathways was likely small in our experiments. For example, in the raw egg white, compared to the sequence we report, the extrapolated proton density was ~4% lower using hard refocusing pulses, and 1% lower with phase encoding and rewinding performed within each echo spacing as in a standard fast spin echo sequence. Together these indicate that refocusing was fairly complete and only limited signal was lost to other pathways. Another factor we have not considered is the dependence of T_2 measurements to echo spacing in a CPMG sequence. In some structures, particularly the fatty yolk, some of the T_2 components may indeed have different values at other echo spacings (14). Further studies addressing the echo spacing dependence of the T2 components would certainly be of interest in this context.

With the limitations discussed above, the 3D CPMG imaging sequence used to acquire the pristine T_2 decay curves achieved in the present work is not clinically feasible since the scan

time, even for the limited volume coverage, was 3 hours. In testing faster methods either based on spin echoes, gradient echoes, combinations of the two, or even steady state methods, having a predictable “gold standard” phantom with well-characterized T_2 decay components mimicking those in myelinated white matter is obviously of value. Dairy cream has been advocated as a phantom for this purpose (15), though the fat/water chemical shift of the two T_2 components may lead to effects not expected in myelin associated water studies, particularly for gradient echo approaches. In contrast, the decay curves from, for example, the HB yolk with fat saturation may prove more useful as there are two water T_2 components, a very rapid (~10 ms) decay and a much slower decay (~100 ms), though the latter is only some 2% of the total contribution to the signal in pure yolk. One can then easily “dial in” a larger second component by simply overlapping the ROI with egg white which has a T_2 value on the order of ~60 ms and so is very similar to the T_2 associated with the water within and between brain cells. Though there will be biological variability among eggs, the basic features of the T2 decay components elucidated above may prove very useful when trying to determine various sequence/parameter factors that affect quantitation of short T2 component measurement. For example, a recent study by Zhang et al (16) determined a significant discrepancy between myelin water fractions in brain as measured via CPMG decay curves vs steady state methods (17). Having the luxury of being able to scan an egg for an unlimited amount of time with different sequences and different parameters to determine potential measurement discrepancies may prove the most valuable use of this phantom. Other recent work has utilized optimized multi-spin echo imaging sequences on clinical 1.5 T systems to demonstrate T_2 decay curves in intact fruit also well-characterized with bi-and/or tri-exponential functions, similar to our findings in the egg (18,19). Given the versatility of T_2 components found in the egg and their relative changes we thus conclude that it could indeed provide a simple and useful “gold standard” phantom for testing more clinically suitable strategies designed to provide information from myelin-associated water.

Acknowledgments

Grant sponsor: National Institute of Biomedical Imaging (S.E.M.), grant numbers: R01 EB006867 and R01 EB010195; **Grant sponsor**: National Cancer Institute (S.E.M.), grant number: R01 CA160902; **Grant sponsor**: National Center for Research Resources, National Cancer Institute, and National Institute of Biomedical Imaging, grant number: R01 U41 RR019703; **Grant sponsor**: National Institute of Biomedical Imaging (D.M.), grant number: K01 EB015868.

REFERENCES

1. Pollan, M. Cooked: A natural History of Transformation. The Penguin Press; NY, NY: 2013.
2. Stadelman, WJ.; Cotterill, OJ. Egg science and technology. The Haworth Press, Inc; Binghamton, NY: 1995.
3. Maier SE, Mitsouras D, Mulkern RV. Avian egg latebra as brain tissue water diffusion model. Magn Reson Med. 2013 doi: 10.1002/mrm.24941.
4. Mitsouras D, Owens CD, Conte MS, Ersoy H, Creager MA, Rybicki FJ, Mulkern RV. In vivo differentiation of two vessel wall layers in lower extremity peripheral vein bypass grafts: application of high-resolution inner-volume black blood 3D FSE. Magn Reson Med. 2009; 62(3):607–615. [PubMed: 19449380]
5. Poon CS, Henkelman RM. Practical T2 quantitation for clinical applications. J Magn Reson Imaging. 1992; 2(5):541–553. [PubMed: 1392247]

6. Bernstein, MA.; King, KF.; Zhou, XJ. Handbook of MRI pulse sequences. Elsevier Academic Press; Burlington, MA: 2004. p. 111
7. Hennig J. Echoes -- how to generate, recognize, use or avoid them in MR-imaging sequences part I: fundamental and not so fundamental properties of spin echoes. Concepts in Magn Reson. 1991; 3:125–143.
8. MacKay A, Whittall K, Adler J, Li D, Paty D, Graeb D. In vivo visualization of myelin water in brain by magnetic resonance. Magn Reson Med. 1994; 31(6):673–677. [PubMed: 8057820]
9. Whittall KP, MacKay AL, Graeb DA, Nugent RA, Li DK, Paty DW. In vivo measurement of T2 distributions and water contents in normal human brain. Magn Reson Med. 1997; 37(1):34–43. [PubMed: 8978630]
10. Whittall KP, MacKay AL, Li DK, Vavasour IM, Jones CK, Paty DW. Normal-appearing white matter in multiple sclerosis has heterogeneous, diffusely prolonged T(2). Mag Reson Med. 2002; 47(2):403–408.
11. Fieremans E, Pires A, Jensen JH. A simple isotropic phantom for diffusional kurtosis imaging. Magn Reson Med. 2012; 68(2):537–542. [PubMed: 22161496]
12. Whittall KP, MacKay A. Quantitative interpretation of NMR relaxation data. J Magn Reson. 1989; 84:134–152.
13. Clark PR, Chuaanusorn W, St Pierre TG. Bi-exponential proton transverse relaxation rate (R2) image analysis using RF field intensity-weighted spin density projection: potential for R2 measurement of iron-loaded liver. Magnetic resonance imaging. 2003; 21(5):519–530. [PubMed: 12878262]
14. Williamson DS, Mulken RV, Jakab PD, Jolesz FA. Coherence transfer by isotropic mixing in Carr-Purcell-Meiboom-Gill imaging: implications for the bright fat phenomenon in fast spin-echo imaging. Magn Reson Med. 1996; 35(4):506–513. [PubMed: 8992200]
15. Jones C, MacKay A, Rutt B. Bi-exponential T2 decay in dairy cream phantoms. Magnetic resonance imaging. 1998; 16(1):83–85. [PubMed: 9436951]
16. Zhang J, Kolind SH, Laule C, Mackay AL. Comparison of myelin water fraction from multiecho T decay curve and steady-state methods. Magn Reson Med. 2014 doi: 10.1002/mrm.25125.
17. Deoni SC, Rutt BK, Arun T, Pierpaoli C, Jones DK. Gleaning multicomponent T1 and T2 information from steady-state imaging data. Magn Reson Med. 2008; 60(6):1372–1387. [PubMed: 19025904]
18. Adriaensen H, Musse M, Quellec S, Vignaud A, Cambert M, Mariette F. MSE MRI sequence optimisation for measurement of bi- and tri-exponential T2 relaxation in a phantom and fruit. Magnetic resonance imaging. 2013; 31(10):1677–1689. [PubMed: 23601362]
19. Winisdorffer G, Musse M, Quellec S, Devaux MF, Lahaye M, Mariette F. MRI investigation of subcellular water compartmentalization and gas distribution in apples. Magnetic resonance imaging. 2015 doi: 10.1016/j.mri.2015.1002.1014.

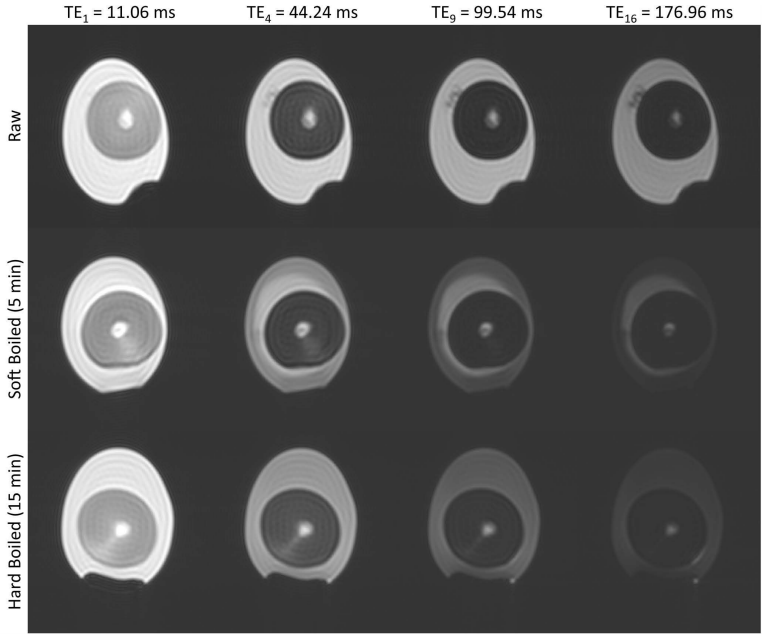

Figure 1.

Sample images through the echo train from one egg at each of the preparation conditions. Gray scale window and level is equal for all images.

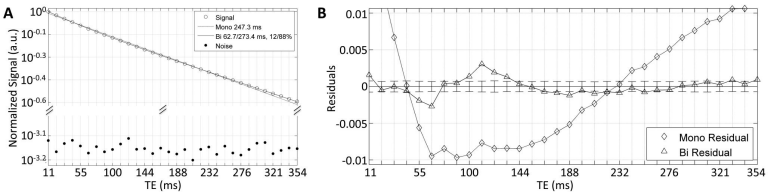

Figure 2.

Signal decay with fits and residuals measured in the egg white of a raw egg. First echo SNRs ranged from 1318 to 2098, and last echo SNRs ranged from 10.6 (SB) to 363.4 (raw). Noise data shown as points in semi-log plot, and as error bars in residual plot indicate the mean signal observed in an empty space ROI.

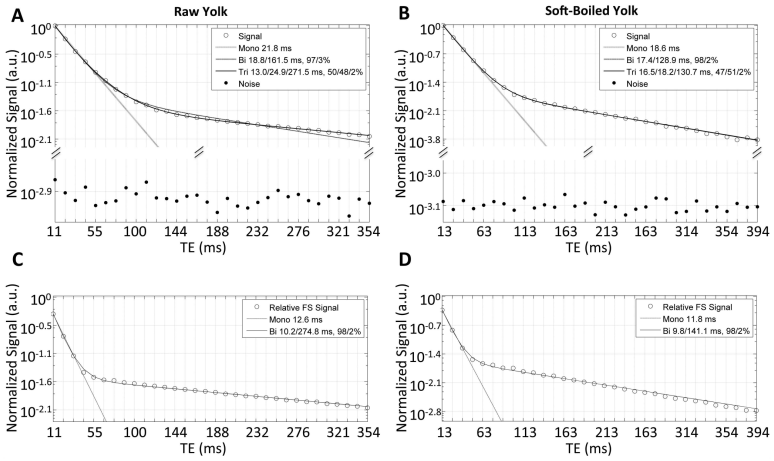

Figure 3.

Signal decays with fits for (**A,C**) raw and (**B,D**) SB egg yolk, shown without (top rows) and with (bottom row) fat saturation (FS) pulse application. Noise data shown is as in Fig. 2. HB yolk (not shown) exhibited similar signal decay as raw yolk.

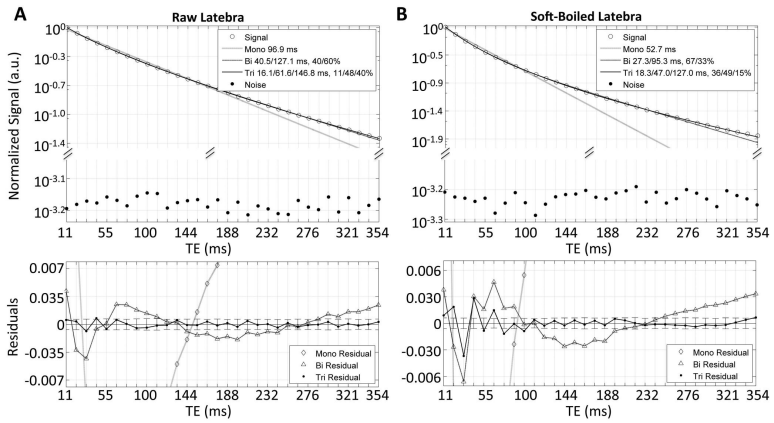

Figure 4.

Signal decays with fits and residuals for raw (**A**) and SB (**B**) latebra. Noise data shown as in Fig. 2.

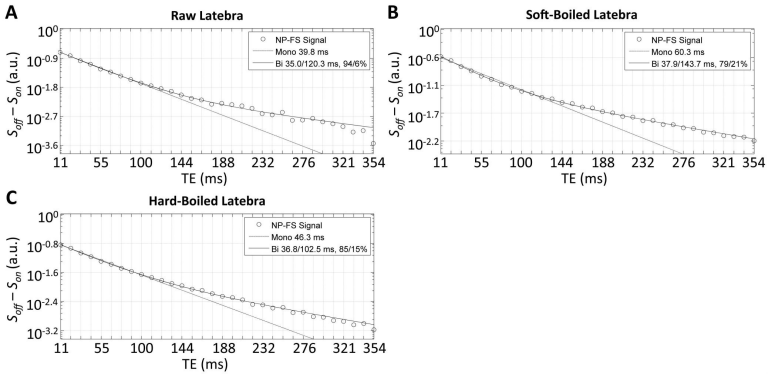

Figure 5.

Signal difference between the NP and FS experiments in the latebra of (**A**) raw, (**B**) SB, and (**C**) HB eggs. Evidently, and as also confirmed by *F*-tests (not shown), the signal difference is better fitted by a biexponential rather than a monoexponential model.

TABLE 1

Relaxation times and relative amplitudes for each structure and condition tested.

		NP		FS	
White					
		Relative Amplitude	Relaxation Time	Relative Amplitude	Relaxation Time
Short T_2	Raw	13.6±1.1%	65.0±3.5 ms	15.7±3.2% *	78.4±8.1 ms *
	SB	33.5±21.1%	41.4±5.5 ms	44.6±23.3% *	44.4±4.5 ms *
	HB	39.6±19.6%	48.3±6.2 ms	42.7±17.8%	49.8±5.1 ms
Long T_2	Raw	86.4±1.1%	217.7±11.4 ms	84.3±3.2% *	224.7±12.0 ms
	SB	66.5±21.1%	61.7±8.1 ms	55.4±23.3%	61.5±6.3 ms
	HB	60.4±19.6%	65.9±6.3 ms	57.3±17.8%	65.8±5.9 ms
Yolk					
		NP		**FS**	
		Relative Amplitude	Relaxation Time	Relative Amplitude	Relaxation Time
Short T_2	Raw	39.2±18.5%	12.6±2.1 ms	96.9±1.4% *	10.8±1.3 ms *
	SB	97.8±0.8%	17.9±0.6 ms	97.3±0.9%	11.6±1.2 ms *
	HB	66.6±2.7%	13.4±0.6 ms	97.2±1.0% *	9.7±0.8 ms *
Intermediate T_2	Raw	58.5±18.3%	23.2±1.7 ms	N/A	N/A
	SB	N/A	N/A	N/A	N/A
	HB	27.0±2.5%	36.5±2.6 ms	N/A	N/A
Long T_2	Raw	2.3±0.9%	288.1±50.9 ms	3.1±1.4% *	295.4±43.1 ms
	SB	2.2±0.8%	104.5±16.4 ms	2.7±0.9%	108.3±21.9 ms
	HB	6.4±2.8%	81.2±9.8 ms	2.8±1.0% *	95.3±5.8 ms *
Latebra					
		NP		**FS**	
		Relative Amplitude	Relaxation Time	Relative Amplitude	Relaxation Time
Short T_2	Raw	24.5±15.5%	15.0±2.2 ms	29.9±21.9%	9.7±2.0 ms *
	SB	33.2±19.4%	18.1±3.1 ms	34.0±20.1%	11.3±1.4 ms *
	HB	23.5±9.2%	18.5±2.5 ms	21.9±5.2%	8.4±1.3 ms *
Intermediate T_2	Raw	46.8±10.4%	49.6±13.3 ms	39.0±10.5%	48.9±15.2 ms
	SB	44.9±7.4%	54.9±5.4 ms	42.4±10.2%	47.7±10.8 ms *
	HB	43.7±3.8%	48.6±6.4 ms	38.8±3.7% *	38.7±3.4 ms *
Long T_2	Raw	28.8±17.9%	134.2±32.2 ms	31.1±19.2%	143.6±35.3 ms
	SB	21.9±13.3%	148.0±16.4 ms	23.6±10.7%	136.6±26.3 ms
	HB	32.8±10.9%	105.4±7.2 ms	39.3±8.0%	99.0±4.8 ms

NP: normal preparation, i.e., neither fat saturation nor magnetization transfer pulses applied. FS: fat-saturation pulse preparation. Statistically significant differences from NP experiment are marked with asterisk

*(). All values are listed with standard deviations across multiple region-of-interest measurements.